IIETA International Information and Engineering Technology Association
Advancing the World of Information and Engineering

Revue des Composites et des Matériaux Avancés-Journal of Composite and Advanced Materials
Vol. 36, No. 3, June, 2026, pp. 553-562
Journal homepage: http://iieta.org/journals/rcma

Experimental Investigation of Cold-Formed Steel Composite Bridge Girder in Various Shapes under Repeated Loads

Ali Allami[1*], Haleem K. Hussain[2], Fareed Hameed Majeed[2]

[1] Department of Civil Technologies, Technical Institute of Amara, Southern Technical University, Misan Governorate 62001, Iraq
[2] Department of Civil Engineering, College of Engineering, University of Basrah, Basrah 61004, Iraq

Corresponding Author Email: ali.allami@stu.edu.iq

Copyright: ©2026 The authors. This article is published by IIETA and is licensed under the CC BY 4.0 license (http://creativecommons.org/licenses/by/4.0/).

https://doi.org/10.18280/rcma.360309

Received: 16 April 2026
Revised: 4 June 2026
Accepted: 19 June 2026
Available online: 30 June 2026

Keywords:
cold-formed steel composite girder, cumulative energy, ductility, experimental study, repeated load test, shapes of cold-formed steel

ABSTRACT

A composite action of a cold-formed steel section and a concrete deck slab depends on the degree of interaction between the steel section girders and the concrete deck slab. In addition to the degree of interaction, the shape of the cold-formed steel section significantly influences the stress distribution of the deck slab under repeated loadings. In this study, all specimens were designed for full interaction and varied in cold-formed section shapes in repeated load tests. Four shapes were investigated in this research: tub, open-box, and double C with and without lips. Four specimens were designed and fabricated to study the flexural and failure behavior of cold-formed steel sections and concrete deck slab in terms of ductility, stiffness, ultimate failure load, crack propagation, residual deflection, and cumulative energy. The experimental results show that the double C-lipped specimen increases the ductility factor by 61%, 36%, and 5% compared to the open box, tub, and double C specimens, respectively. Additionally, the residual deflection of the double C-lipped specimen was lower during the repeated loading stages, whereas the tub specimen recorded a higher value. The results indicated that the cumulative energy of the double C-lipped specimen was the highest value.

1. INTRODUCTION

Cold-formed steel section composite bridge girders have been suggested as a viable solution to reduce the construction time and costs of bridge design and construction [1-6]. The cold-formed steel composite girder is transported to the bridge site following full prefabrication. Prefabrication is a common way in bridge engineering that involves the prefabrication and on-site assembly of certain bridge components, hence reducing costs for cutting and welding plates. The composite bridge girder consists of a cold-formed steel section and a precast or cast-in-place RC slab connected to the steel section by shear connectors. The steel section girder is being manufactured with a high-capacity press-brake. Plates are positioned in the press-brake and cold-bent to get the specified bend radius. Another method of cold-formed composite girder construction is prefabrication [5, 7].

The study of the cold-formed plate girder system under static load tests began in 1978, when Kennedy et al. [8] designed a full-scale composite bridge girder using cold-formed steel and an RC deck slab. Additionally, Taly and Gangarao [9] proposed a new T-Box bridge girder system utilizing a composite tub girder fabricated from a steel plate bent by a press brake, along with an experimental investigation under static load testing. Nakamura [10] studied the positive and negative bending moments of a new composite bridge girder under static load. Folded Plate Girder (FSPG) System (see Figure 1(a)) was studied and developed under static load testing [1, 11-13] and fatigue load testing [14]. Recently, Kelly [15] tested non-composite press-brake-formed steel tub girders (PBFTG). The experiment used two non-composite girders. Short-span bridge shallow PBFTG were invented by Barth et al. [16]. Michaelson's girder consists of a press-brake-formed steel tub section and a cast-in-place RC deck joined by shear studs, as shown in Figure 1(b). Tumbeva et al. [17] developed a novel approach to the production of cold-formed tub composite girders. A built-up steel tub girder system was constructed with a web that was cold-formed and attached to top flanges and flat bottom plates. Morgan [18] investigated the flexural behavior of PBFTG under low-skew angles to improve their applicability.

The investigation of the cold-formed plate girder system under repeated or fatigue load tests started in 2010, when Burner [14] studied the performance of the composite FSPG system under the action of fatigue loading. To investigate the behavior of joints between attached slabs, six slab specimens with closure areas were subjected to both positive and negative moments. The fatigue loading was carried out by subjecting the girder to a 75-year lifetime loading equivalent. Kozhokin [19] studied a trapezoidal box girder with a joint made of ultra-high-performance concrete (UHPC), reaching a strength of 24 ksi (165 MPa). UHPC was used to create sturdy joints

connecting the trapezoidal box girders. The composite tub girder system consists of two composite box girders jointed with UHPC and subjected to fatigue loads. Gibbs [7] conducted a field behavior evaluation on a press-brake-formed steel tub com. Tennant [3] investigated how the uncoated and galvanized press-brake-formed composite tub performed during fatigue loading. Tennant [20] focused on developing the cold-formed steel tub girder system, which was performed in several steps. An experimental fatigue test was applied to the two PBFTGs linked by a joint slab to evaluate the joint in continuously press-brake-formed tub girders. Studies [5, 21-23] investigated the live load distribution factors for press-brake-formed tub girder bridges in the field and analytically.

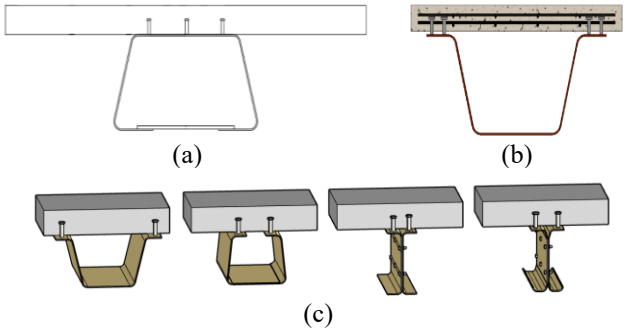

Figure 1. Cold-formed steel composite girder proposed by (a) Michaelson [24], (b) Burner [14], and (c) present study

Two innovative girder designs for short-span bridges have been derived from prior research on cold-formed steel concrete composite girders: the folding plate girder system and the cold-formed steel tub girder. Allami et al. [25] investigated the influence of shape on the static structural performance of cold-formed composite girders. No research has been undertaken regarding the influence of shape on the repetitive structural performance of cold-formed composite girders in short-span bridges. Four cold-formed shapes were developed, manufactured, and subjected to experimental repeated load testing to assess the performance of the cold-formed composite bridge girder in terms of ductility, stiffness, ultimate failure load, crack propagation, residual deflection, and cumulative energy (see Figure 1(c)).

2. EXPERIMENTAL DESIGN

2.1 Specimen design

The design of the composite girder was completed by determining the characteristics of each selected shape. Reducing assumptions regarding the capacity of the composite girder allows the completion of design iterations [24]. Michaelson [24] and Allami et al. [25] outline the design process used to determine the optimal depth for each shape. Due to their usefulness in cold-formed girder systems and steel bridges, tub sections, open box sections, double C-sections, and double C-lipped sections were selected.

The yield moment of each specimen at different depths establishes the optimum depth for each shape. The shapes and dimensions used in this study were similar to the shapes chosen for the static load test by Allami et al. [25] (refer to Table 1 and Figure 2). Figure 3 illustrates the flowchart of the experimental work in this study.

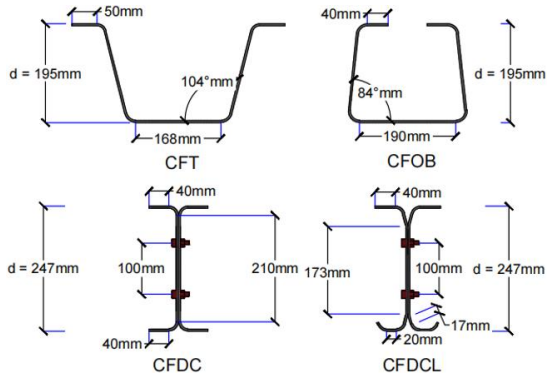

Figure 2. Cold-formed steel shapes of composite girders used in the present study

Table 1. Design comparison of cold-formed composite girders (yield moment M_y in kN·m at selected depths)

Specimen Designs	100 mm	150 mm	195 mm	250 mm
CFT	-----	111.5	112.0	105.0
CFOB	108.1	117.3	119.5	118.7
CFDC	80.83	92.4	107.1	113.9
CFDCL	80.70	92.7	106.8	115.0

Note: CFT = Cold-Formed Tub; CFOB = Cold-Formed Open-Box; CFDC = Cold-Formed Double C; CFDCL = Cold-Formed Double C Lipped.

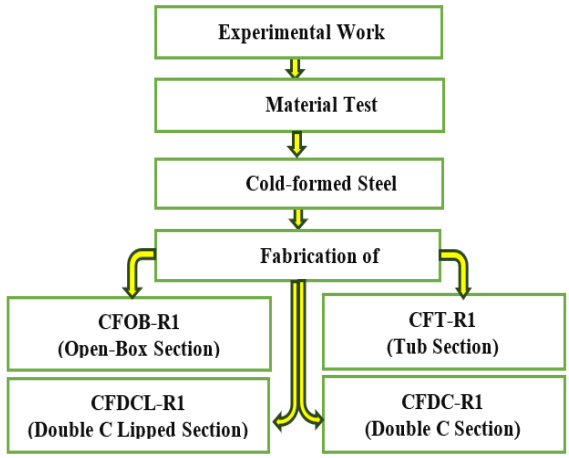

Figure 3. Flowchart of the experimental work in the present study

Table 2. Cross-sectional properties of proposed cold-formed composite girders

Specimens	A, mm^2	t, mm	d, mm	S_{xx}, mm^3	Shape of Section
CFT-R1	2800	4	195	364683	Tub
CFOB-R1	2800	4	243	367727	Open-Box
CFDC-R1	2800	4	195	350629	Double C
CFDCL-R1	2800	4	247	353871	Double C Lipped

Note: A = area of cross-section of steel, t = thickness of steel section, d = total depth of specimen, S_{xx} = section modulus; CFT = Cold-Formed Tub; CFOB = Cold-Formed Open-Box; CFDC = Cold-Formed Double C; CFDCL = Cold-Formed Double C Lipped.

To assess the impact of cross-sectional shape on structural behavior under repeated load testing, an experimental program was specifically designed as a comparison study. Similar specimens of a steel section, as suggested by Allami et al. [25], were utilized in this investigation. The deck slab was 500 mm wide and 100 mm thick, and each specimen had a span length

of 3 m. Table 2 and Figure 4 provide specifics on the cross-section specimens utilized in the present study.

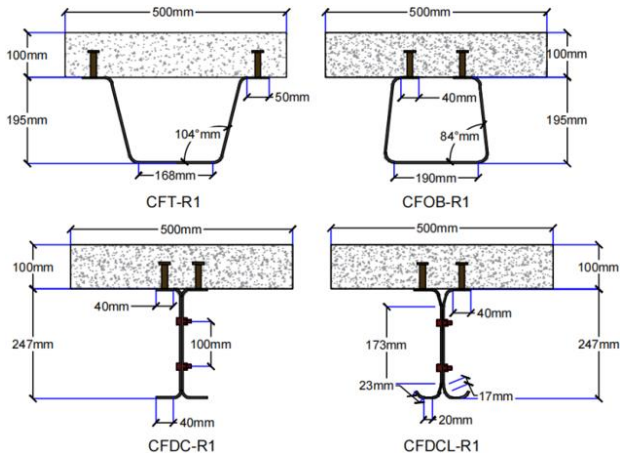

Figure 4. Shapes and dimensions of the cold-formed steel concrete girders (t = 3.7 mm)

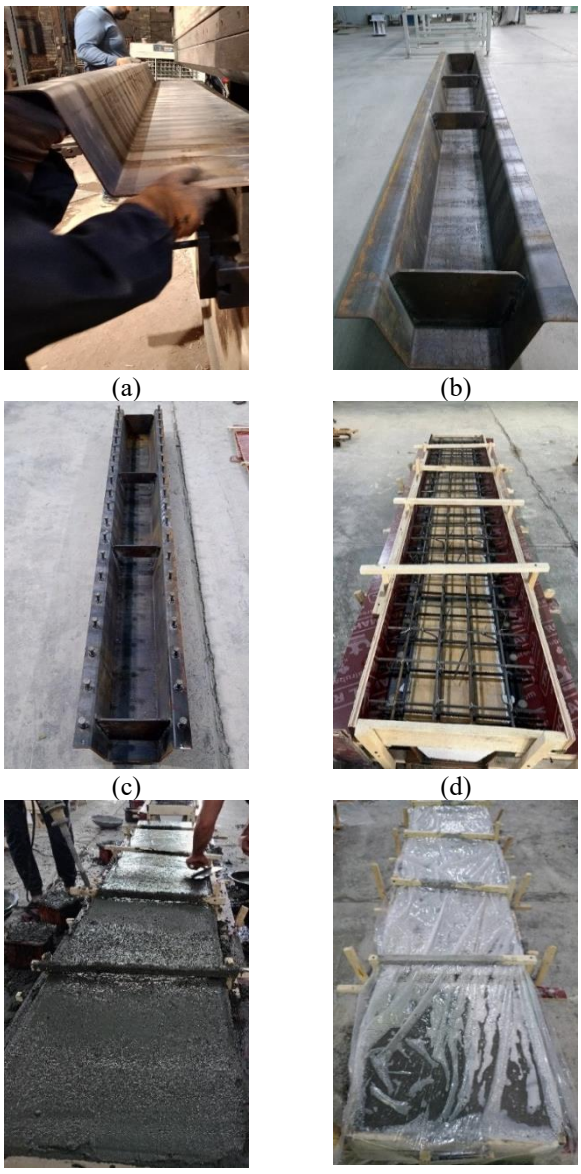

Figure 5. Specimens fabrication: (a) cold-formed plate, (b) welding the stiffeners plate, (c) welding the shear studs, (d) formwork and reinforcement, (e) casting, and (f) curing

A single steel plate with dimensions of 3000 mm × 700 mm × 3.70 mm was used to fabricate each specimen of the cold-formed steel girder. Figure 5(a) shows the use of a high-capacity bending press brake for forming four specimens from the plate. The plates are cold-formed to the specified bending radii after being placed in the press-brake machine. Figure 5(b) shows the welding of a stiffener plate at the supports and point loads to delay bearing failure during the repeated test. Full interaction design of specimens based on AASHTO 6.10.10. 4.1.2. Each top flange was welded with a single row of shear studs measuring 12.75 mm × 60 mm, spaced at 150 mm, for a total of 20 studs per specimen, as shown in Figure 5(c). After the steel girders' fabrication was finished, the reinforcement of the deck and wood forms was placed around the specimen (see Figure 5(d)). The specimens were left in place after the concrete pouring was completed and cured in water for 28 days (see Figure 5(e) and (f)). The deck slab reinforcement was designed according to the empirical deck approach described in section 9.7.2 of the AASHTO LRFD standard (AASHTO 2010) [26] (see Figure 6). After completing the curing, the specimens were painted and prepared for testing, as shown in Figure 7. The connection between the double C-section was created with a two-row bolt (diameter 4.8 mm) spacing of 200 mm (see Figure 8).

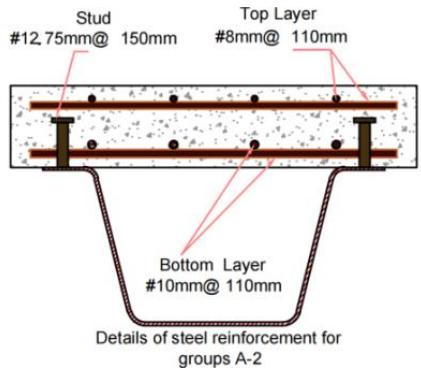

Figure 6. Deck reinforcement for specimens

Figure 7. Painted specimens ready for testing

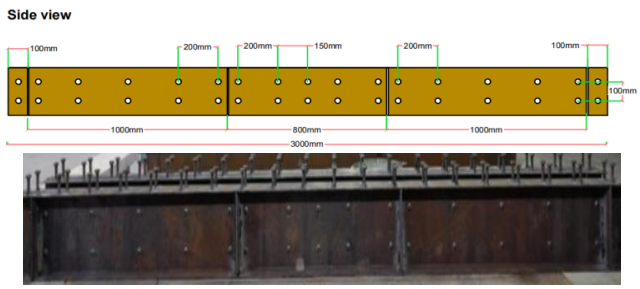

Figure 8. The connection of the specimens using bolts

2.2 Material properties

Based on the properties of the materials, the ACI 211 specification [27] is used to design the concrete mix. Various trial batches of the concrete mix design were cast to obtain the necessary compressive strength. Final mixing quantities were as specified in Table 3.

The compressive strength of each specimen was determined by casting three cubes of standard-weight concrete, as described in references [28, 29]. The specimens and the cubes were tested concurrently, and the mean concrete compressive strength for all cubes was 36.60 MPa.

Three specimens of steel reinforcement for each diameter, measuring 500 mm in length, were tested in accordance with ASTM A615/A615M-22 [30] at the Construction Laboratory of the Technical Institute of Amara. Table 4 presents the characteristics of the samples evaluated for each of the steel plates [31], rebar reinforcement, and shear stud.

Table 3. Contents of the concrete mix

Cement, kg/m^3	Fine Aggregate, kg/m^3	Coarse Aggregate, kg/m^3	Water, kg/m^3	W/C Ratio
430	725	930	194	0.45

Note: W/C Ratio = Water-to-Cement Ratio.

Table 4. The average properties of the samples tested

Sample	Yield Strength, MPa	Tensile Strength, MPa	Elongation, %
Rebar 8 mm	568	665	13
Rebar 10 mm	559	699	11
Stud 12.75 mm	350	432	24
Steel plate 3.7 mm	335	419	28

2.3 Experimental set-up and loading programs

A load was applied with an MTS 600-kN servo-hydraulic actuator. The dimensions and testing arrangement are shown in Figure 9. The testing starts with the documentation of the preliminary measurements from the load and strain gauges, followed by the incremental application of the load. At each phase, the data logger records the measurements from the load and strain gauges, the appearance of cracks is documented, and markers are applied to designate their positions.

The linear variable displacement transducers, low-voltage deflection devices (LVDTs), were employed to determine the vertical deflections, with each transducer having a total range of 100 mm. The mid-span depth of the girder was measured at four levels using strain gages, as illustrated in Figure 10.

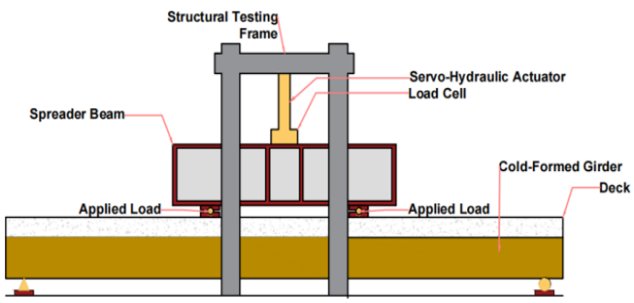

(a)

(b)

Figure 9. (a) Typical test setup layout, (b) isometric view of a standard test setup

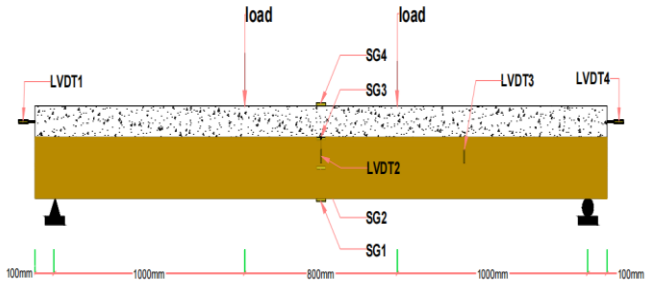

Figure 10. A strain gauge location at four levels across the section depth of the specimen

Tokyo Measuring Instruments Laboratory (TML) strain sensors and a GEODATALOG 8 data recorder were employed to conduct the measurements. One strain gauge was mounted to the top of the concrete surface, while three were set up along the bottom steel flange, top steel flange, and web of the girder. Repeated tests were conducted on composite girders of cold-formed steel section and concrete deck slab in the construction laboratory of the Technical Institute of Amara at Southern Technical University. An MTS 600-kN servo-hydraulic actuator machine was used for repeated loading tests. The support was a simply supported girder under a four-point load and subjected to the same testing conditions. Repeated load tests were performed on four specimens at loads equal to 75% and 85% of the ultimate load from the static test by Allami et al. [25]. A total of 200 cycles were applied, including 130 cycles at 75% of the ultimate load and 70 cycles at 85% of the ultimate load. The load was then applied statically and gradually increased until it failed. The repeated loads were applied in two patterns based on the ultimate loads from the static test [25]: pattern A was used for specimens CFT-R1 and CFOB-R1, while pattern B was used for samples CFDC-R1 and CFDCL-R1, as shown in Figure 11. The test method was carried out in force-controlled mode. Each loading cycle lasted 4 minutes, from the beginning of loading to the highest peak load of 0.75% pu and 0.85% pu kN. The specimen was then fully unloaded, with a minimum load of about zero. The unloading phase and the subsequent inter-cycle rest interval before the start of the next cycle were rigorously limited to 60 seconds, respectively, to allow for possible elastic recovery of the specimen. This loading approach was performed consistently for 200 cycles (as shown in Figure 11) for all models under the identical conditions to assess the periodic response data properly. Data were recorded and documented every 10 cycles using a data logger to record the strain and deflection at the mid-span and ends of specimens.

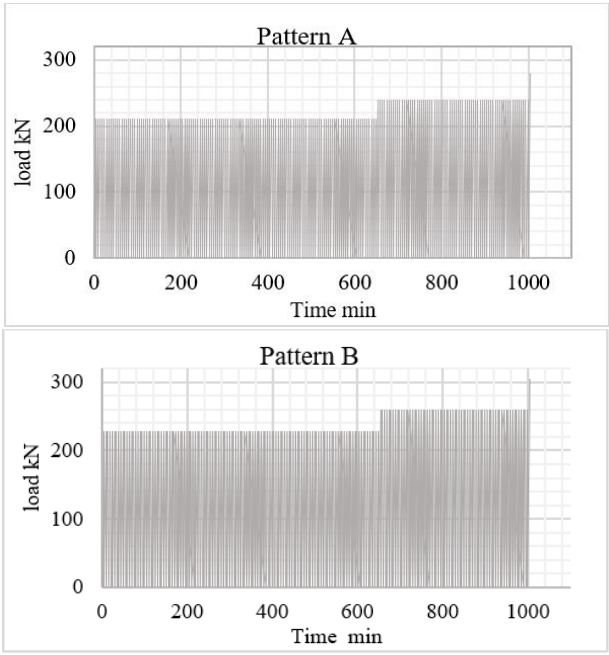

Figure 11. The applied loading of specimens in repeated tests (200 cycles)

3. EXPERIMENTAL RESULTS AND DISCUSSION

3.1 Failure modes

The failure mode of the specimens was the crushing of the concrete in the mid-span of the upper deck slab of the girder. After completing 200 cycles, the specimens did not fail, but cracks appeared at various stages. The first crack appeared in the CFT-R1 girder at a load of 205 kN in the first cycle, and with an increase in the number of cycles at a load of 75% (210 kN), more cracks propagated at the bottom of the deck slab. More cracks appeared when the second stage of cycles (85% of the ultimate load (239 kN)) was applied at primary cycles. After completing the 200 cycles, the specimen was loaded statically to failure at 289 kN load. The failure mode of the CFT-R1 specimen under the repeated load test is similar to the static test [25], with more cracks appearing. Figure 12 shows the failure mode of the specimens after completion of the testing. At the first cycle of the 210 kN load (75% of the ultimate load), no cracks appeared in the deck slab of the CFOB-R1 specimen. As the number of cycles increased, cracks appeared, albeit to a lesser extent than in the CFT-R1 model. With the primary cycles of the second stage (which represents 85% of the ultimate load of 239 kN), more cracks were observed. After completing 200 cycles, the specimen was loaded statically to failure at 281.6 kN load. The failure mode was crushing of the concrete in the upper part of the deck slab.

For the CFDC-R1 and CFDCL-R1 specimens, the applied load was 228 kN, instead of 210 kN for cycles, which is equivalent to 75% of the ultimate load, representing a 9% increase. Additionally, the load increased by 8.63% for cycles of 85% of the ultimate load, reaching 259 instead of 239. This increase was due to the higher ultimate load observed in static testing [25]. The CFDC-R1 and CFDCL-R1 specimens propagated less than the CFT-R1 and CFOB-R1 specimens under the cyclic load (85% of the ultimate load). After completing 200 cycles, the specimens were loaded statically to failure. The ultimate loads for CFDC-R1 and CFDCL-R1 were 314.1 kN and 334.2 kN, respectively, which increased the number of cracks in the mid-span of the specimens. Figure 13 shows the specimens after completing the test.

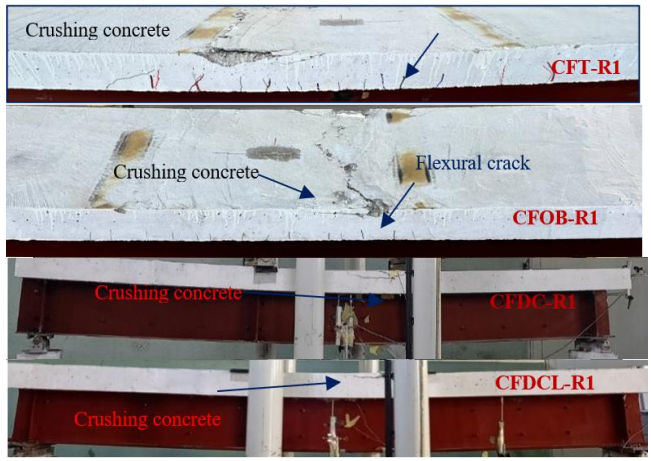

Figure 12. Failure modes of specimens

Figure 13. The specimens after completing the test

3.2 Load-deflection curve of specimens

The load-deflection curve of the composite bridge girder allows for characterization of its behavior as either brittle or ductile. The stiffness is defined as the slope of the load-deflection relationship [32] as described by the following equation:

$$stiffness(kN/mm) = \frac{\delta\, p}{\delta\, \Delta} \quad (1)$$

The stiffness of specimens is calculated by dividing the difference between peak and minimum load by the difference in deflection at the peak and minimum point loads after 130 and 200 cycles of repeated loading. Figures 14-18 illustrate the load-deflection curve of specimens, with deformations monitored using LVDTs. The curves consist of three phases: the first is a 130-cycle load applied at 75% of the failure load, the second is a 70-cycle load applied at 85% of the ultimate load, and the final phase involves static loading to failure. The specimens were in the elastic-plastic phase when loaded statically after repeated loading, and the deflection increased most rapidly. The load-deflection curve for the CFOB-R1 specimen indicates early failure to its ultimate load capacity, in contrast to the other specimens (Figure 15). The use of double C-sections increased the cross-sectional stiffness and ductility at mid-span before failure.

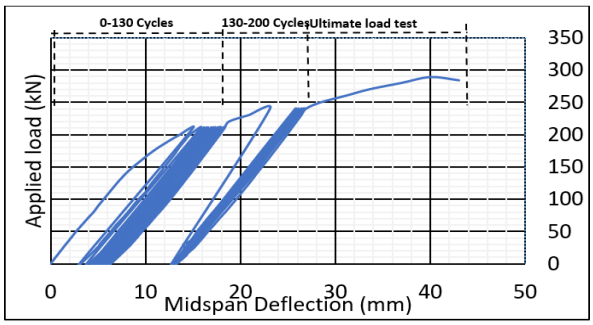

Figure 14. Load-deflection curve of CFT-R1 specimen under repeated load test
Note: CFT = Cold-Formed Tub.

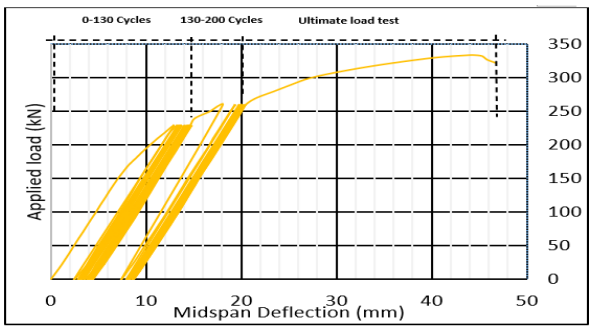

Figure 17. Load-deflection curve of CFDCL-R1 specimen under repeated load test
Note: CFDCL = Cold-Formed Double C Lipped.

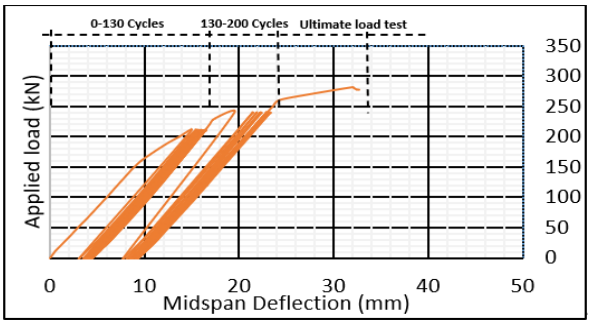

Figure 15. Load-deflection curve of CFOB-R1 specimen under repeated load test
Note: CFOB = Cold-Formed Open-Box.

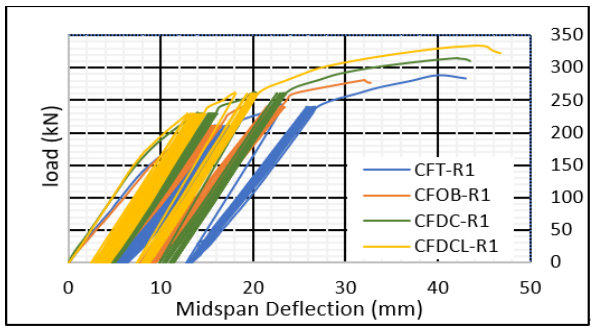

Figure 18. Load-deflection curve of specimens under repeated load test

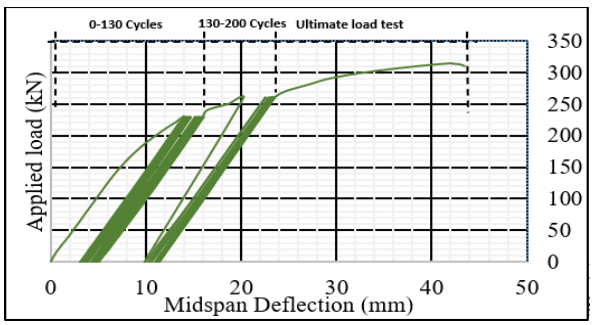

Figure 16. Load-deflection curve of CFDC-R1 specimen under repeated load test
Note: CFDC = Cold-Formed Double C.

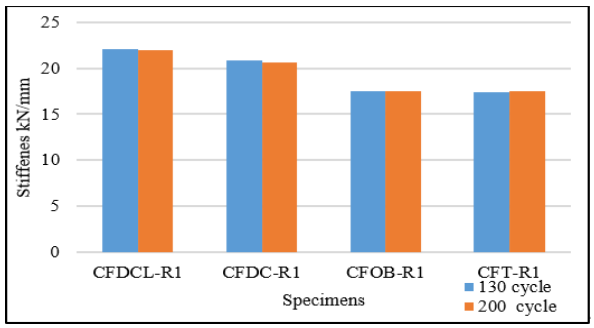

Figure 19. Stiffness of specimens under repeated loading
Note: CFT = Cold-Formed Tub; CFOB = Cold-Formed Open-Box; CFDC = Cold-Formed Double C; CFDCL = Cold-Formed Double C Lipped.

Table 5. Results of the repeated test of Group B

Stiffens after 200 Cycles	Ultimate Load, kN	Ultimate Deflection, mm	Yield Load, kN	Yield Deflection, mm	Specimen
17.51	289	38	240.1	13.70	CFT-R1
17.52	281.6	32.068	240.1	13.70	CFOB-R1
21.50	314.1	42.039	260.2	11.77	CFDC-R1
22.10	334.2	44.418	260.2	11.77	CFDCL-R1

Note: CFT = Cold-Formed Tub; CFOB = Cold-Formed Open-Box; CFDC = Cold-Formed Double C; CFDCL = Cold-Formed Double C Lipped.

Table 5 shows the yield load, ultimate load and stiffness after completing the repeated loading and reloading to failure load. The stiffness variations of the tested specimens were minimal over the 200 cycles (see Figure 19). The stiffness results for the CFDC-R1 and CFDCL-R1 specimens showed similar values under a peak load (259 kN), as well as for the CFT-R1 and CFOB-R1 specimens at a load of 239 kN (see Figure 18). The stiffness was enhanced by 26 % when using the CFDC-R1 and CFDCL-R1 specimens compared to the CFT-R1 and CFOB-R1 specimens.

3.3 The ductility factor of specimens

The results of repeated load tests showed different values of the ductility factor after 200 cycles. A load-deflection curve after repeated loading was adopted to calculate the ductility factor of the specimens (see Figure 20).

The ductility factor is calculated by dividing the deflection at the failure load value by the deflection value at yield load, as described by the following equation [33, 34]:

$$Ductility\ factor = \frac{deflection\ at\ ultimate\ load}{deflection\ at\ yield\ load} \quad (2)$$

The ductility factor of the four specimens from the repeated load test is shown in Table 6. Repeated tests of specimens revealed that the CFDCL-R1 specimen had the greatest ductility factor, which was 3.77. The ductility factor of CFOB-R1 was the lowest value, equal to 2.34, and it failed early. The CFDCL-R1 specimen increases the ductility factor by 61%, 36%, and 5% compared to the CFOB-R1, CFT-R1, and CFDC-R1 specimens, respectively.

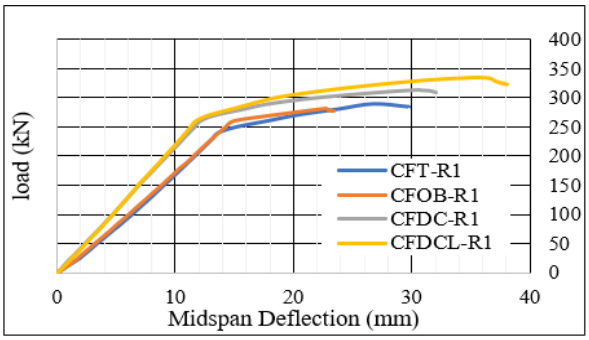

Figure 20. Load-deflection curve of specimens after completion of the number of cycles, then loading to failure

Table 6. Ductility factor of specimens

Specimen	CFT-R1	CFOB-R1	CFDC-R1	CFDCL-R1
Ductility factor	2.77	2.34	3.57	3.77

Note: CFT = Cold-Formed Tub; CFOB = Cold-Formed Open-Box; CFDC = Cold-Formed Double C; CFDCL = Cold-Formed Double C Lipped.

3.4 Strain of specimens

3.4.1 The strain of the concrete deck slab

The strain of the concrete deck slab was measured using strain gauges installed on its surface, denoted SG4. The load-strain curves were recorded at the top of the concrete deck slab for three stages: first, after 130 cycles; second, after 200 cycles; and third, at the ultimate loaded stage as the repeated loading progressed (see Figure 21).

The load value obtained at a strain of 0.00076 rose from 281.6 kN to 315 kN when the CFDCL-R1 specimen was used instead of the CFOB-R1. Furthermore, the load value for the CFDC-R1 specimen increased to 310 kN. This increases the capacity by 11.86% and 9.16% in the CFDCL-R1 and CFDC-R1 specimens, respectively, as compared to the CFOB-R1 specimen.

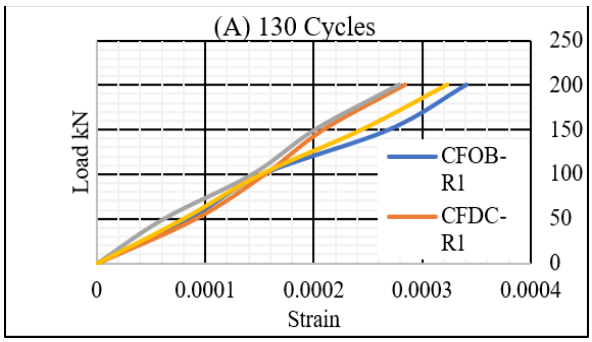

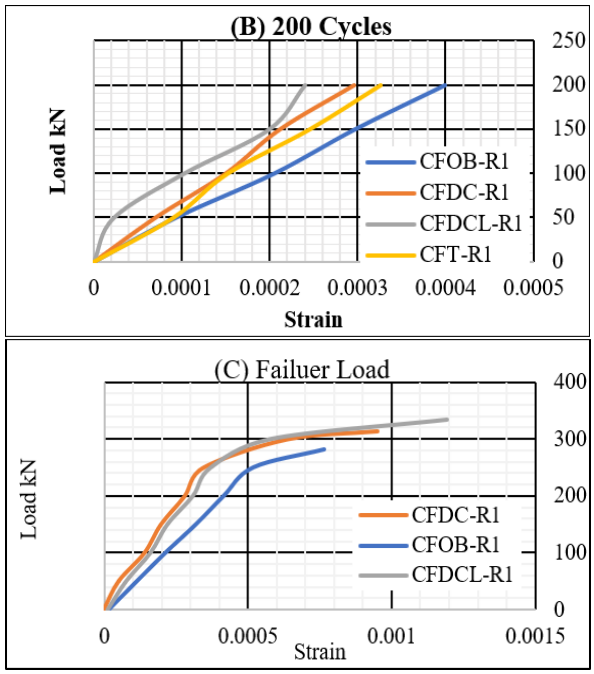

Figure 21. Strain results of specimens at the top deck slab concrete (SG4) after 130 cycles (A), 200 cycles (B), and at failure load (C)

3.4.2 The cold-formed steel section strain

The strain distribution along the cold-formed steel section was recorded during the cycles of the repeated tests. Figures 22 and 23 show typical strain results of the specimens in the bottom flange and web for three stages of the repeated tests. The cold-formed steel section at strain gauge positions SG1, SG2, and SG3 was generally in tension, while the deck slab concrete of strain gauge SG4 was in compression.

Based on the mechanical properties of the steel plate listed in Table 4, all strain values presented in Figures 22 and 23 were below the yield point at the repeated loading stage. As the repeated cycle progressed, the strains were linear and fairly uniform at the bottom flange of the steel section, as shown in Figure 22.

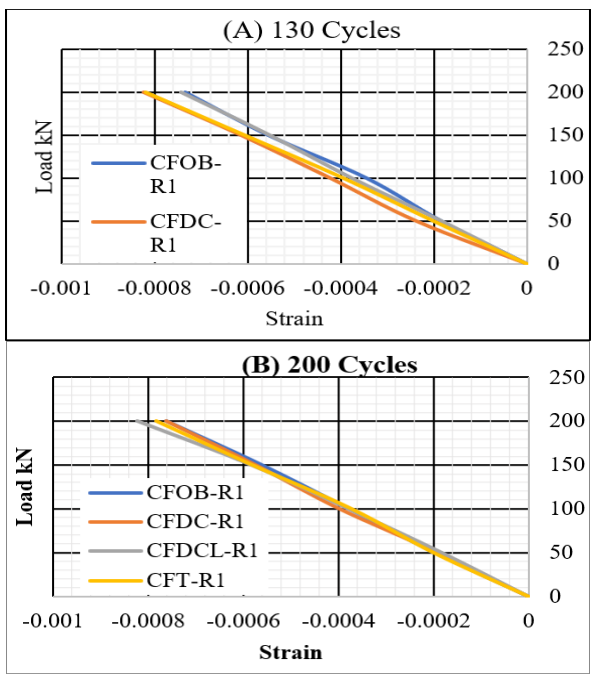

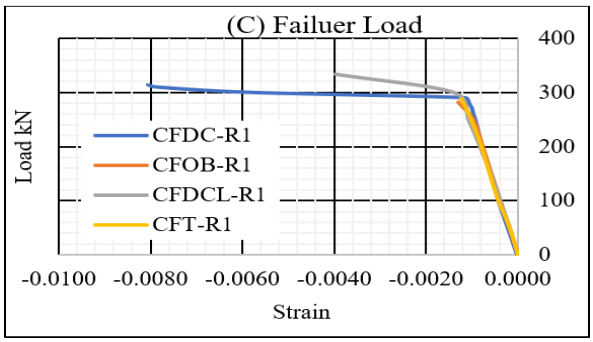

Figure 22. Strain results of specimens at the bottom steel flange (SG1) after 130 cycles (A), 200 cycles (B), and at failure load (C)

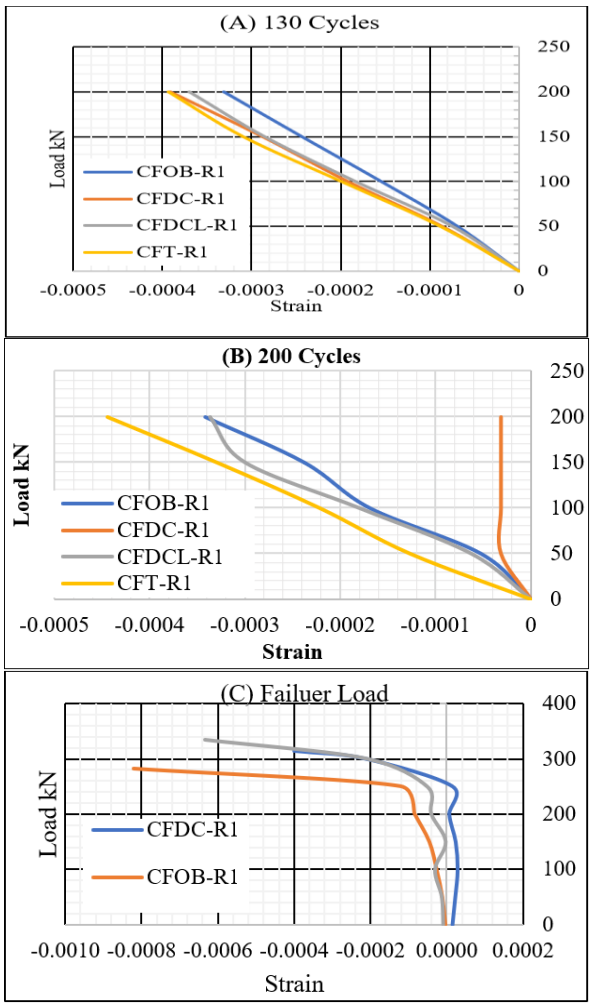

Figure 23. Strain results of specimens at the steel web (SG2) after 130 cycles (A), 200 cycles (B), and at failure load (C)

In the ultimate load testing, after completing repeated cycles, both CFT-R1 and CFOB-R1 specimens failed in crushing concrete at the top deck slab. In comparison to the CFDC-R1 and CFDCL-R1 specimens, both demonstrated higher endurance at the same recorded strain, as illustrated in Figures 21(A)-(C), essentially attributable to enhanced structural performance. When utilizing the CFDCL-R1 specimen, the load value at a strain of 0.000396 increased from 281.6 kN to 343 kN compared to the CFDC-R1 specimen, indicating enhancements of 21.63%.

In comparison to the CFOB-R1 specimen, the load values of the CFDCL-R1 and CFDC-R1 specimens increased from 265 kN to 317 kN and 310 kN, respectively, at a strain of 0.00063, indicating enhancements of 19.62% and 16.98% for the CFDCL-R1 and CFDC-R1 specimens in the web steel section (SG2) (see Figure 23). The strain was recorded for the top flange steel part, denoted SG3. Strain values recorded were small at the top flange during repeated loading and at the ultimate load test.

3.5 Residual deflection

Residual deflection in a composite bridge girder denotes the measured deflection remaining in the bridge girder after the removal of applied repeated loads. This deflection represents the permanent deformation resulting from the plastic behavior of the steel section and concrete, as well as the weakness of the surface connection between the concrete and steel sections. These factors may decrease its practicality in the future and increase the possibility of concrete cracks or separation at the steel-concrete interface. LVDTs are used to measure the residual deflection to monitor deformations for each cycle. The residual deflection was recorded every 10 cycles, except for the initial ten cycles, which were all recorded.

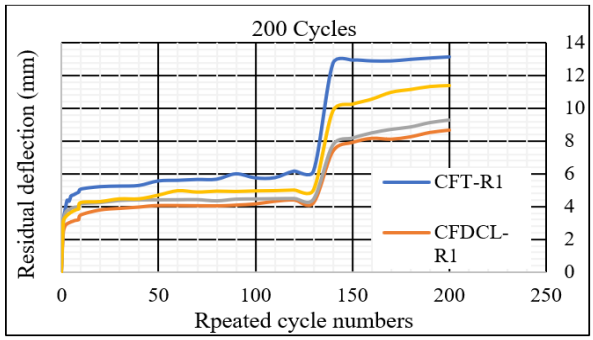

Figure 24. Residual deflection of the specimens under repeated load

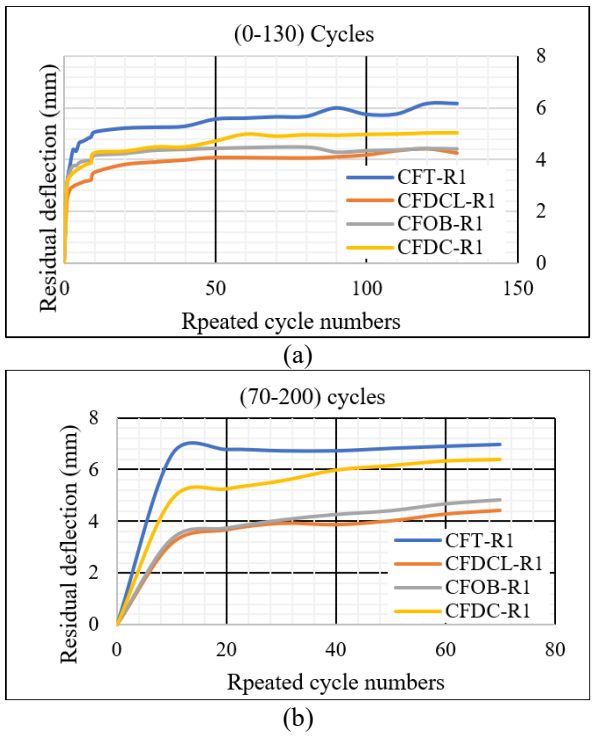

Figure 25. Residual deflection of the specimens at mid-span after (a) 130 cycles and (b) 200 cycles

Figures 24 and 25 present the residual deflections of the specimens after 130 and 200 loading cycles, respectively. The CFDCL-R1 specimen showed a lower residual deflection during the repeated loading test. This value was 51%, 31%, and 7% lower than those of the CFT-R1, CFDC-R1, and CFOB-R1 specimens, respectively.

3.6 Cumulative energy

Cumulative energy is an important measure in analyzing the cyclic behavior of the composite bridge girder of a cold-formed steel section and concrete deck. It signifies the cumulative energy absorbed by a structural system across repeated loading and unloading cycles. This energy includes both the recoverable stored elastic energy and the unrecoverable plastic energy dissipated through permanent deformations and structural fatigue. With continuous cyclic loading, cumulative energy increases, indicating a gradual loss of component characteristics, including flexural stiffness and the bridge's capacity to dissipate loads efficiently. The Cumulative energy is equivalent to the area under the cyclic tangent load-deflection curve of 200 cycles until load failure (see Figures 14-17).

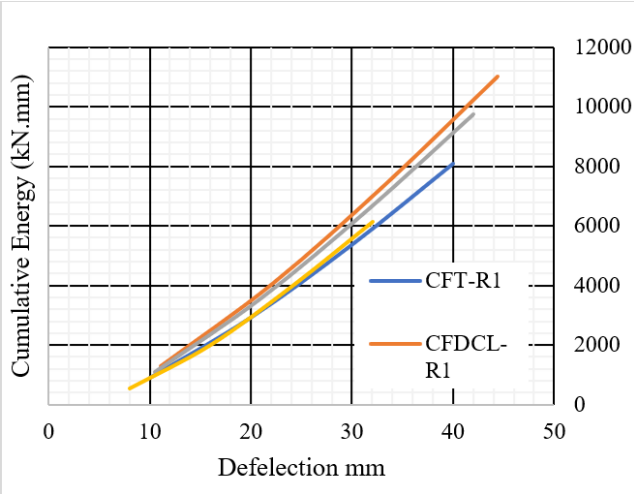

Figure 26. Cumulative energy of the specimens in repeated loading

The experimental results revealed a roughly linear connection between accumulated energy and deflection in the early stages. Followed by an apparent expansion of energy reduction as the structural failure approached (Figure 26). The results indicated that the cumulative energy at failure for the CFDCL-R1 specimen, after completing the specified number of load cycles, was the highest value, exceeding that of the CFDC-R1, CFT-R1, and CFOB-R1 specimens by 16%, 36%, and 60%, respectively. The CFOB specimen had the lowest value and failed at an early stage due to the deck slab being exposed to higher strain during the repeated loading cycles. The increase in cumulative energy signifies a shift from elastic to ductile behavior. Cumulative energy analysis can provide initial indications of structural performance deterioration under repeated loads.

4. CONCLUSIONS

The primary objective of this study is to investigate the repetitive behavior of cold-formed steel composite girders with various shapes under four-point static loading. Four simply supported girder specimens were designed, fabricated and tested under repeated loads. The study investigated the effect of various cold-formed steel section shapes on the performance of composite bridge girders in terms of ductility, stiffness, ultimate failure load, residual deflection, and cumulative energy. Several conclusions can be listed as follows within the tested specimens:

1. The use of double C-lipped can effectively improve the cross-sectional stiffness. Additionally, enhance the ductility factor at mid-span by 61%, 36%, and 5% compared to the open box, tub, and double C specimens, respectively.
2. The double C-lipped specimen exhibited 36% lower residual deflection compared to the tub specimen after 200 loading cycles.
3. The load capacity obtained at the same level of strain in the deck slab concrete and bottom steel flange is improved when the double C-lipped section is used instead of the open box section.
4. The results indicated that the cumulative energy at failure for the double C-lipped specimen after the given number of load cycles was higher by 80% than that of the open box specimen.

In summary, the double C-lipped section specimen gets higher stiffness and ultimate load capacity, performs better in terms of ductility, and has the greatest cumulative energy value after completing the required number of repeated load cycles.

ACKNOWLEDGMENT

This work was partially supported by Southern Technical University under scientific research awards, No. 9/7934, 10 Sep. 2025.

REFERENCES

[1] Civjan, S.A., Sit, M.H., Breña, S.F. (2016). Field and analytical studies of the first folded-plate girder bridge. Journal of Bridge Engineering, 21(11): 04016074. https://doi.org/10.1061/(ASCE)BE.1943-5592.0000918

[2] Barth, K.E., Michaelson, G.K., Tennant, R.M. (2020). Fatigue performance of singular and modular press-brake-formed steel tub girders. Bridge Structures, 16(1): 3-13. https://doi.org/10.3233/BRS-200168

[3] Tennant, R.M. (2018). Fatigue performance of uncoated and galvanized composite press-brake-formed tub girders. Master's thesis. West Virginia University. https://doi.org/10.33915/etd.6783

[4] Deng, Y., Phares, B.M., Steffens, O.W. (2016). Experimental and numerical evaluation of a folded plate girder system for short-span bridges–A case study. Engineering Structures, 113: 26-40. https://doi.org/10.1016/j.engstruct.2016.01.027

[5] Barth, K.E., Michaelson, G.K., Roh, A.D., Tennant, R.M. (2021). Field determined live load distribution factors for modular press-brake-formed tub girders. Transportation Research Record, 2675(3): 1-7. https://doi.org/10.1177/0361198120983757

[6] Hameed, M., Almayah, A.A., Naser, K.Z. (2025). A state

of the art on composite steel-reactive powder concrete structures. Civil Engineering Science and Technology Journal, 1(1): 77-83.

[7] Gibbs, C.L. (2017). Field performance assessment of press-brake-formed steel tub girder superstructures. Master's thesis. West Virginia University. https://doi.org/10.33915/etd.5671

[8] Kennedy, J.B., Madugula, M.K., Keen, R.G., Fung, C. (1978). Cold-formed steel in composite bridge construction. Canadian Journal of Civil Engineering, 5(2): 164-173. https://doi.org/10.1139/l78-021

[9] Taly, N., Gangarao, H.V.S. (1979). Prefabricated press-formed steel T-box girder bridge system. Engineering Journal, 16(3): 75-83. https://doi.org/10.62913/engj.v16i3.337

[10] Nakamura, S.I. (2002). Bending behavior of composite girders with cold formed steel U section. Journal of Structural Engineering, 128(9): 1169-1176. https://doi.org/10.1061/(asce)0733-9445(2002)128:9(1169)

[11] Burgueño, R., Pavlich, B.S. (2008). Evaluation of prefabricated composite steel box girder systems for rapid bridge construction (Research Report No. CEE-RR – 2008/01). Michigan State University.

[12] Azizinamini, A. (2009). A new era for short-span bridges. Steel Bridge News, p. 20. National Steel Bridge Alliance. https://www.aisc.org/media/vqehh0ng/msc_article_reprint2009.pdf.

[13] Glaser, L.A. (2010). Constructability testing of folded plate girders. Master's thesis. University of Nebraska–Lincoln. http://digitalcommons.unl.edu/civilengdiss/9.

[14] Burner, K.A. (2010). Experimental investigation of folded plate girders and slab joints used in modular construction. Master's thesis. University of Nebraska–Lincoln. https://digitalcommons.unl.edu/civilengdiss/8/.

[15] Kelly, L.T. (2014). Experimental evaluation of non-composite shallow press-brake-formed steel tub girders. Master's thesis. West Virginia University. https://doi.org/10.33915/etd.5958

[16] Barth, K.E., Michaelson, G.K., Barker, M.G. (2015). Development and experimental validation of composite press brake–formed modular steel Tub girders for short-span bridges. Journal of Bridge Engineering, 20(11): 04015007. https://doi.org/10.1061/(asce)be.1943-5592.0000770

[17] Tumbeva, M.D., Mutoka, S.C., Thrall, A.P., Zoli, T.P., Wagner, S., Baah, P. (2023). Built-up press brake-formed tub girders. Journal of Bridge Engineering, 28(12): 04023092. https://doi.org/10.1061/jbenf2.beeng-6103

[18] Morgan, M.L. (2024). The impact of low-skew on the ultimate capacity of press-brake-formed tub girders. Master's thesis. West Virginia University. https://doi.org/10.33915/etd.12456

[19] Kozhokin, P. (2016). Evaluation of Modular press-brake-formed tub girders with UHPC joints. Master's thesis. West Virginia University. https://doi.org/10.33915/etd.6010

[20] Tennant, R.M. (2022). Expanding the applicability of press-brake-formed tub girders through the extension of the maximum span length and the evaluation of pier continuity. Ph.D. dissertation. West Virginia University. https://doi.org/10.33915/etd.11405

[21] Woldegabriel, B.T. (2023). Development and validation of improved live load distribution factors for moment in press-brake-formed steel tub girder bridges. https://doi.org/10.33915/etd.12197

[22] Barth, K.E., Michaelson, G.K., Pyrialakou, V.D., Woldegabriel, B.T., Mason, J.R., Tennant, R.M. (2025). Enhancing live load distribution predictions for press-brake-formed tub girder bridges for moments in interior girders: A statistical approach. Journal of Bridge Engineering, 30(6): 04025025. https://doi.org/10.1061/jbenf2.beeng-6440

[23] Barth, K.E., Michaelson, G.K., Pyrialakou, V.D., Woldegabriel, B.T., Tennant, R.M. (2025). Applicability and validation of improved live load distribution factors for commercially available shallow steel tub girders. Bridge Structures, 21(2-3): 81-92. https://doi.org/10.1177/15732487251330406

[24] Michaelson, G.K. (2014). Development and feasibility assessment of shallow pressbrake-formed steel tub girders for short-span bridge applications. Ph.D. dissertation. West Virginia University. https://doi.org/10.33915/etd.6227

[25] Allami, A., Hussain, H.K., Majeed, F.H. (2026). Experimental study of cold-formed steel bridge girder in various shapes under static loads. Civil Engineering Journal, 12(3): 1190-1204. https://doi.org/10.28991/CEJ-2026-012-03-021

[26] American Association of State Highway and Transportation Officials (AASHTO). (2010). Guide Specifications for Seismic Isolation Design (Third Edition).

[27] Wilson, J.R. (1974). Recommended practice for selecting proportions for no-slump concrete. Journal of the American Concrete Institute, 71(4): 153-170.

[28] BS EN 12390-1:2021. (2001). Testing hardened concrete–Part 1: Shape, dimensions and other requirements for specimens and moulds. BSI Standards Publication.

[29] BS EN 12390-3:2009. (2009). Testing hardened concrete compressive strength of test specimens. BSI Standards Publication.

[30] ASTM A615/A615M -22. (2024). Standard specification for deformed and plain carbon-steel bars for concrete reinforcement. ASTM International, West Conshohocken, PA, USA. https://store.astm.org/a0615_a0615m-22.html.

[31] ASTM A370-17. (2017). Standard test methods and definitions for mechanical testing of steel products. ASTM International, West Conshohocken, PA, USA. https://store.astm.org/a0370-17.html.

[32] AL-Farttoosi, H.K.A., Hussain, H.K., Abdulrazzaq, O.A. (2021). Flexural behavior of two-layer beams made with normal and lightweight concrete layers. Periodicals of Engineering and Natural Sciences, 9(2): 1124-1140. https://doi.org/10.21533/pen.v9.i2.814

[33] Huang, Q., Liu, Y., Guo, Z., Ju, J.W.W. (2025). Flexural fatigue strength of RC bridge girders strengthened by PHSW-PM. Engineering Structures, 338: 120640. https://doi.org/10.1016/j.engstruct.2025.120640

[34] Ahmed, A.S., Al-Fahal, A.S., Al-Hantoosh, N.M., Hussein, M.A. (2024). Static load behavior of ferrocement slabs reinforced with recycled tire steel wire. Revue des Composites et des Materiaux Avances, 34(1): 117. https://doi.org/10.18280/rcma.340115